One-Dimensional Oxide Nanostructures: Growth, Applications and Devices

S. Barth, S. Mathur, F. Hernandez-Ramireza, A. Romano-Rodrigueza

Dem immer wieder geäußerten Wunsch nach einem stärkeren Engagement des INM im NanoBioNet wurde seit Ende 2005 Rechnung getragen. Schließlich wählte die Mitgliederversammlung im Dezember 2007 Jochen Flackus zum Vorsitzenden des Vereins.

Beide Kompetenzzentren, cc-NanoChem und NanoBioNet, haben sich auf ihren jeweiligen Mitgliederversammlungen 2007 für eine engere Zusammenarbeit der Vereine ausgesprochen, wobei auch die Möglichkeiten einer Fusion evaluiert werden sollen.

Leibniz-nano!

Innerhalb der Leibniz-Gemeinschaft forschen eine Reihe von unterschiedlichen Instituten an nanotechnologischen Themenstellungen auf hohem Niveau. Im vorangegangenen Jahr wurde daher der Wunsch nach einer engeren Zusammenarbeit innerhalb der Gemeinschaft artikuliert und am INM die Koordinierungsstelle Nanotechnologien der Leibniz-Gemeinschaft eingerichtet.

Um eine effiziente Vernetzung zu gewährleisten, wurde von Anfang an auf persönliche Kontakte gesetzt. Die beteiligten Institute haben jeweils einen kompetenten Ansprechpartner für die Nanoaktivitäten im Hause benannt, die Anfang 2007 von Herrn Dr. Schubert vor Ort besucht wurden. Auf der Liste der Institute standen neben dem INM zunächst das IKZ in Berlin, das INP in Greifswald, das IHP in Frankfurt (Oder), das ISAS in Dortmund und Berlin, das FZD in Dresden, das IOM in Leipzig und das FIZ in Karlsruhe. Die beiden Dresdner Institute IPF und IFW kamen Mitte des Jahres dazu. Auch hier wurde bei einem Besuch der persönliche Kontakt aufgebaut. Damit hat die Koordinierungsstelle einen guten Überblick über die Aktivitäten und Kompetenzen der Partner.

Eines der zentralen gemeinsamen Ziele ist es, die Sichtbarkeit der WGL zu erhöhen. Ein Schritt in diese Richtung war die konzentrierte Beteiligung am Stuttgarter MiNaT-Kongress. Nicht nur in der Zahl der Beiträge konnte sich die WGL gegenüber den anderen Wissenschaftsgesellschaften behaupten. Auch im Marketing der Veranstaltung fand das Logo der Leibniz-Gemeinschaft seinen Platz neben Frauenhofer-Gesellschaft, Max-Planck-Gesellschaft und Helmholzgemeinschaft.

Auch gemeinsame Messeauftritte sind für die Zukunft geplant. So haben sich INP und INM bereits über den gemeinschaftlichen Auftritt auf der Hannover Messe 2008 verständigt.

One-Dimensional Oxide Nanostructures: Growth, Applications and Devices

One dimensional (1D) inorganic materials are gaining high attention due to their structural stability and unique structural features[1]. Among them, oxides are widely studied due to their well established application potential and mechanical as well as chemical stability. We have deve-

loped a generic approach for size-selective and site-specific growth of oxide nanowires by combination of a catalyst assisted growth mechanism and a molecular precursor approach, which is a viable alternative to other gas phase and solution procedures and produces well-defined (morphology and composition) materials.

Tin Oxide Nanowires

We reported the size-selective synthesis of tin oxide NWs in earlier studies, which allowed the investigation of diameter-dependent photo-conductance with nanowire diameters in the range of 50-1000 nm[2]. In addition, the stable response over several on-off cycles demonstrated their potential as photo detectors[2].Besides multiwire devices, individual tin oxide wires, contacted by FIB nanolithography, were investigated via a combination of two- and four-probe geometries towards their electrical properties[3]. An alternative strategy to FET measurements was described to evaluate conductivity σ_2, charge carrier density η_d and mobility μ in SnO_2 NWs circuits.[4] However, self heating effects and metrological precautions should be taken into account in order to prevent destruction or degradation of these devices as shown in figure 1.

Resistive-type metal oxide sensor, such as tin oxide, uses surface chemical reactions and the subsequent transduction of its electronic properties (e.g., change in the density of conduction band electrons or valence band holes) to detect various gaseous species[5]. However selectivity of SnO_2 surfaces towards atmospheric moisture and water vapor (H_2O) greatly influences their application as reliable gas sensing devices[6]. Since electrical response of SnO_2 nanostructures critically depends on pre-adsorbed species at the oxide surface, understanding the role and influence of water vapour in sensing mechanism is essential for the optimization of phenomenological experiments and more importantly in evaluating the potential of tin oxide-based devices[7]. The interfering effect of water vapor has been investigated in some cases, for example in the detection of carbon monoxide (CO), however the different interaction mechanisms of H_2O molecules and SnO_2 surface are only vaguely described.[7] Heiland and Kohl proposed a widely accepted model of the metal oxide surface interaction with water molecules[8]. A realistic interaction model between water and SnO_2 should, however, consider the effects introduced by chemisorbed oxygen at the surface of the metal oxide. Henrich and Cox proposed a displacement of pre-adsorbed oxygen by water adsorption[9], which was supported by reliable hints for an influence of water vapor on oxygen chemisorption found by several groups. Similarly, Caldararu et al. assumed the blocking of oxygen absorption sites by water molecules[10]. All these mechanisms describe the major role surface states play in the interaction of metal oxide and H_2O.

We have performed humidity sensing experiments close to the temperature (~ 300 °C) required for the detection of carbon mono-

xide, which is one of the most prominent applications of SnO_2-based sensors[11]. More than 10 % variation in the sensor resistance values was observed when water vapor pulses with concentrations as low as 1400 ppm (equivalent to 5 % humidity at 25°C) were introduced in N_2 atmosphere at 295°C. Up to 80 % variation in the resistance values were obtained after injection of water vapor pulses equivalent to 100 % of humidity at 25°C in Standard Atmosphere. The electrical response (change of resistance) can be approximated by the following power law outlined in eq. 1

$$R = R_0 (1 - [H_2O]^{\beta}) \qquad (1)$$

where R_0 is the NW resistance in dry nitrogen or pure synthetic air, $[H_2O]$ the water vapor concentration (in ppm units), and β a constant parameter. A double-logarithmic plot of the sensor response, shown in figure 2, revealed a linear dependence of device responses on water vapor concentration.

The electrical change, which is directly related to the concentration of the water vapor pulses, is almost the same in SA and N_2 experiments. It must be pointed out that the relative resistance difference under N_2 and SA atmospheres is almost constant with similar β values ($\beta(N_2) = 0.21$, $\beta(SA) = 0.19$), which suggests that the water molecules adsorb on the coordination sites and do not necessarily compete with pre-adsorbed species. However, a chemical reaction of H_2O molecules upon increasing concentration with the adsorbed oxygen species (O^{2-}, O^- and O^{2-}) can not be ruled out.[12] Finally, the sensor stability was evaluated as function of operating time, where none of the measured NWs was damaged after several operating cycles. In addition, no significant changes in their sensing capabilities were observed after one month in open air atmosphere, which suggested that a long lifetime and trustworthy responses could be expected for these components.

In order to fabricate portable devices based on individual nanostructures SnO_2 nanowires were contacted to microelectrodes on free-standing micromembranes by FIB nanolithography techniques. The electrical characterization was performed using an electronic circuit designed to prevent the destruction of such devices due to uncontrolled current fluctuations. Modulation of the device temperature was shown to be reproducible and fast due to the integrated heater on the micromembranes. The obtained devices showed stable and reproducible responses for different CO concentrations demonstrating their potential as gas sensors. The article dealing with this topic was selected by the journal Nanotechnology as one of the hot papers and cover page (figure 3) [13].

Alignment of SnO_2 NWs on surfaces was achieved by controlling the lattice mismatch between NW material and substrate ($(aSnO_2 - aTiO_2) / aTiO_2 = 2.6$ % and $(cSnO_2 - cTiO_2) / cTiO_2 = 7.7$ %). The aligned growth of SnO_2 nanowires was achieved by catalyzing the nucleation of one-dimensional nanostructures through gold nanoparticles, and exploi-

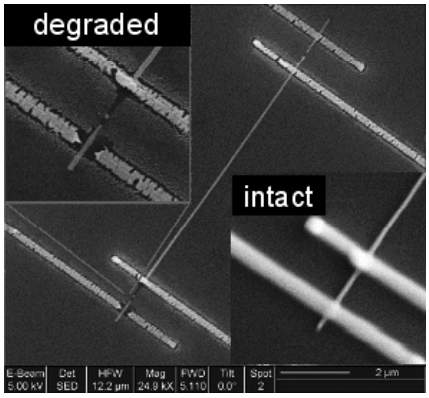

Figure 1: FIB nanolithography fabricated circuit based on an individual SnO_2 NW showing intact and degradated electrical contacts.

ting the structural relationship between TiO_2 and SnO_2 systems. Since the lattice parameters of tin and titanium oxides showed considerable mismatch (up to 7.7 %), the interface needs to relax to accommodate the strain [14]. In-plane SEM view of tin oxide NWs confirmed an oriented growth with a mesh-like network of straight NWs of regular dimensions (figure 4). The diameters of oriented as-grown NWs ranged from 15-25 nm and the length was typically found to be in the range 0.5 - 5 µm. Cross-sectional view in scanning electron microscope (SEM) revealed a characteristic angular orientation of NWs with respect to the substrate, presumably imposed by the four-fold axis of symmetry present along the c-axis in TiO_2 (001) substrate, which offered the growing tin oxide nanowires four equivalent growth directions due to mirror images of the unit cell. In order to elucidate the influence of substrate orientation on observed growth, TiO_2 (100) was also used to grow SnO_2 NWs (figure 4b), which resulted in two main growth directions and appearance of secondary alignment effects, caused by the substitution of equivalent sides with low lattice mismatch (a-axis 2.6 %) through c-axis orientation (7.7 %). Figure 4c reveals randomly oriented NW nucleation on (111)-oriented TiO_2, where the lattice mismatch is too large to favour NW alignment.

High-resolution TEM images of several tin oxide nanowires revealed that the majority of them exhibited preferred growth along <031> direction, which contrasts

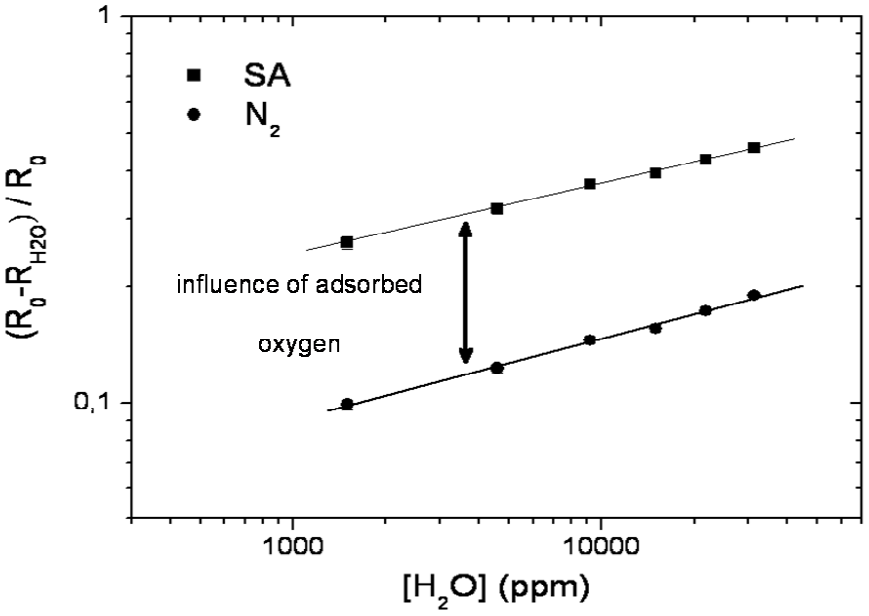

Figure 2: Double logarithmic plot of the response of an individual SnO_2 NW (r = 50 nm) to different humidity concentrations in SA and N2 environments. An offset introduced by ionosorbed oxygen contribution in SA atmosphere is observed.

the expected growth axis (<001>) based on the crystallographic relationship between the substrate and the NW material. This could be caused by an energetically favoured growth axis, with contributions of the bulk energy of tin oxide, the bulk energy of the liquid droplet, the interfacial tension of the liquid solid interface and the surface tensions of the droplet and the nanowire, respectively [15].

Despite proven experimental strategies for site-selective growth of NW ensembles, numerical control over lateral density of NWs remains a crucial challenge. The Au-catalyzed growth of nanowire arrays was downsized to grow individual NW by depositing gold colloids on TiO_2 (001) substrates using spin-on tech-

Figure 3: Portable SnO_2 NW device (inset) developed in collaboration with University of Barcelona was featured on the cover page of the journal Nanotechnology (2007, Vol. 18, 495501) [13].

niques. Controlled decomposition of the precursor at 700°C on individually dispersed Au nanoparticles provided singly grown NWs with growth axis identical to that found in NWs grown in bundles. In addition to oriented nanowires, the rest of the substrate was covered with a nanocrystalline film (figure 5) illustrating the competing catalyzed (1D) and uncatalyzed (2D) growth. Selectivity of the nanowire growth is limited by the fact that only a fraction (approximately 30-70 %) of catalyst particles act as growth initiators. A similar observation has been recently made in vertically oriented Ge nanowires grown from gold colloids on silicon substrates [16]. The observation that the density of gold colloids is not comparable to the density of nanowires may relate to several factors such as the surface charge (due to citrate ions present on Au particles) and agglomeration, which may influence the activity and melting point of the gold nanoparticles, respectively.

Iron oxide (Fe3O4)

Nanoscaled iron oxides are promising for magnetic (e.g., spintronics) and manifold biomedical applications such as drug delivery [17, 18], gene therapy [17, 19], hyperthermic cancer treatment [17, 20], and contrast agents in magnetic resonance imaging (MRI) [17, 21]. When compared to large body of data available on synthesis, characterisation and applications of magnetic nanoparticles [20], reports on anisotropic nanostructures such as nanowires and nanotubes are limited to templated [22], hydrothermal [23], and catalyst-assisted pulsed laser deposition processes[24] as well as reduction of pre-grown α-Fe_2O_3 [25].

CVD of $[Fe(O^tBu)^3]^2$ enabled the formation of 1-D magnetite nanostructures at temperatures between 750-850 °C. The thermal fragmentation of Fe^{3+} species under low pressure partially reduced Fe^{3+} to Fe^{2+} leads to the formation of nanostructured magnetite films at elevated temperatures (figure 6) [26]. The phase purity of the as-obtained nanostructures was investigated by XRD analysis, which exhibited a pure Fe_3O_4 composition devoid of other Fe:O phases. Deposition on MgO (100) had an aligning effect on the growing structures, which is suited for growing highly oriented magnetite coatings due to its low lattice mismatch (0.3 %) with Fe_3O_4 [27] and produced both wiry and saw-like morphologies [28].

Four equivalent growth orientations evident in SEM images (figure 7a), indicated the influence of crystallographic relationship between the oriented substrate and magnetite nanostructures. Figure 7b shows transmission electron microscope (TEM) images of straight (figure 7a) and zigzag magnetite nanostructures (inset). Both, HR-TEM and corresponding FFT images revealed the single crystalline nature of the 1D magnetite nanostructures. Interplanar spacings and corresponding FFT revealed the preferred growth direction to be <110> (figure 7c). Lattice spacings of 0.2980 nm match well with the (220) lattice planes of magnetite (0.2967 nm, PDF 19-0629). The catalyst particle was clearly identified as a globu-

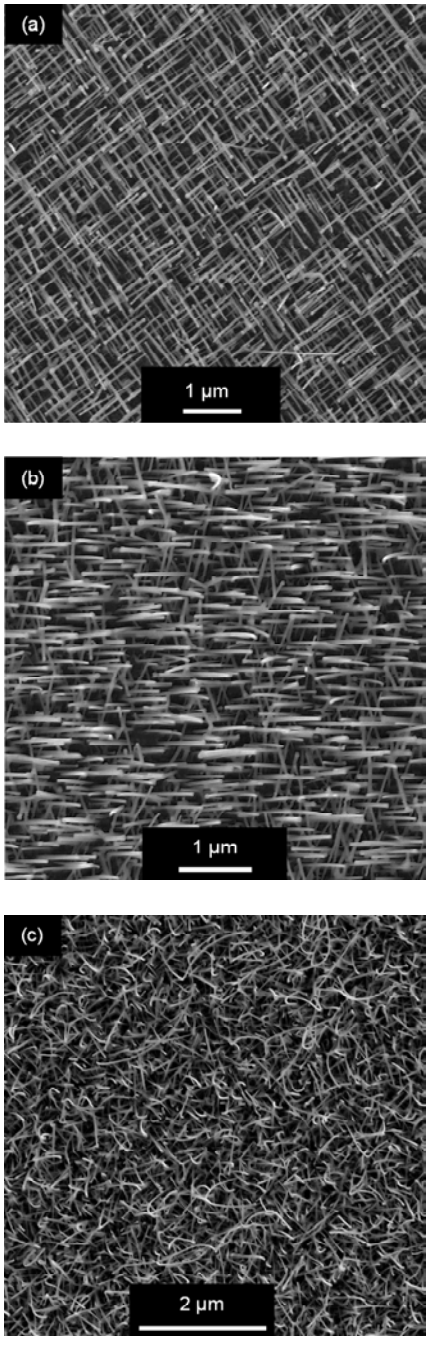

Figure 4: SnO_2 NWs on single crystalline TiO_2 substrates of (a) (001), (b) (100) und (c) (111) orientation.

lar tip, whereby the gold metal was found to align with the cubic oxide structure providing a coincidence grain boundary, where the (111) planes of Au align along the (220) lattice planes of Fe_3O_4 and the resulting strain at the interface is relaxed through one dimensional defects. During the course of the CVD process, growth of new 1 D structures via catalyst-assisted mechanism and further growth on initially formed nanowires, supported through layer-by-layer growth was observed, which resulted in stepwise tapered structures (figure 7b).

Formation of facets due to kinetic barriers is common in the gas phase growth of crystalline materials. If the deposition rates do not vary substantially the diffusion kinetics of adatoms is determined by the diffusion distances and the associated kinetic barriers on flat surfaces and near surface steps. Apparently, the migration along <110> step edge is thermodynamically favoured and thus fast diffusion path for the atoms, which limits the formation of flat surface and leads to the pronounced formation of facetted nanostructures as observed in figure 7b. As a result both axial and radial dimensions of the nanowires grow during the CVD process, due to competing catalyst-assisted growth occurring at the nanowire tip and diffusion-assisted growth active on the nanowire body.

Individual magnetite NWs were contacted to Pt electrodes using FIB nanolithography procedures, as described in literature [12]. I-V characteristics were investigated in two point configuration. The observed ohmic response of this device could be attributed to metallic conduction of the Fe_3O_4 NW at 300 K. The resistivity value was in the range of ~9 10^{-6} Ω•m, which is in the range of reported data for single crystals.[29] Two out of three measured devices showed resistivities in the range of 9-10 10^{-6} Ω•m, however high contact resistance contributions must be taken into account, which was already described for FIB contacts to SnO_2 NWs.[4]

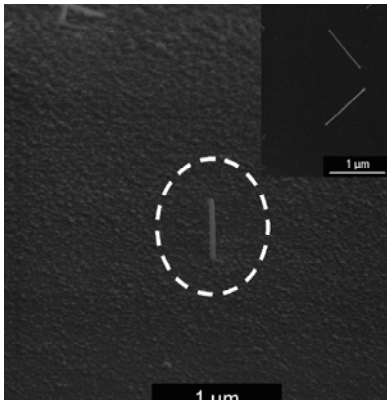

Figure 5: SEM image of an individual SnO_2 NW grown on TiO_2 (001) surrounded by a nanocrystalline film (picture taken under 30° angle to the substrate surface) and plane view of oriented grown wires (inset).

1D Oxide Heterostructures

In order to grow longitudinal heterostructures, SnO_2 nanowires formed by the CVD of $Sn(O_{Bu}{}^t)_4$ [2] were used as substrates to obtain tin oxide/magnetite nanostructures (figure 8). We have synthesized SnO_2/Fe_3O_4 core-shell structures by a two-step growth process, where initially grown tin oxide NWs (∅ 50 nm) were covered by a dense assembly of magnetite nanocrystals forming a polycrystalline layer (figure 8a), which was confirmed by X-ray diffraction analysis. Sub-

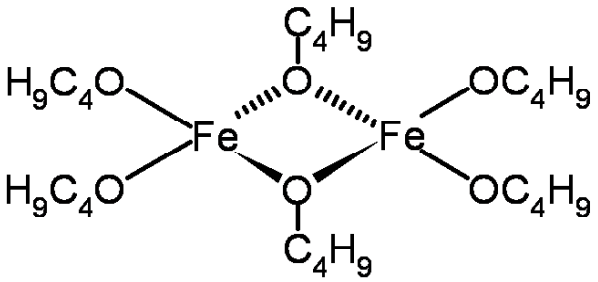

$$[Fe(OtBu)_3]_2 \longrightarrow \text{“}FeO_x\text{”} + x\,(CH_3)_3COH + y\,(CH_3)_2CCH_2 + z\,H_2$$

Figure 6: Molecular structure of $[Fe(O^tBu)^3]^2$ and scheme of the thermally activated decomposition in a CVD process.

ject to the precursor flux and adjustment of CVD parameters, the magnetite shell sometimes connected several pre-formed crossed NWs of the SnO_2 substructure to form interconnected magnetite superstructures with several junctions at the micro-scale. Differences in electrical and magnetic properties between single crystalline wires and polycrystalline core-shell structures are currently underway.

Branched one-dimensional heterostructures were fabricated by growing vanadium oxide nanostructures on pre-grown SnO_2 backbones by decomposition of [VO(O^iPr)3]. Hierarchical structures involving second generation growth of nanowires, have been realized using a sequential two-step strategy. Merely few data exists in the literature dealing with epitaxial growth of a high axial ratio oxide nanostructure on a one-dimensional oxide host structure possessing different chemical compositions and crystal structures [30]. This is a generic approach and should in principle provide access to various combinations of materials especially in systems where an intrinsic doping is not possible due to solubility limitations. Hierarchical growth exhibiting strong interaction of individual vanadium oxide sub-structure with the tin oxide backbone was observed in 1D and 2D configurations (parallel or/and normal to tin oxide NW axis). The geometrical features of the V_2O_5 nanostructures were modulated by varying the precursor flux (temperature), whereby elongated structures were formed at higher gas phase saturation. HR-TEM images of SnO_2-V_2O_5 interface revealed a strong alignment of the two different crystal lattices, resulting in a heteroepitaxial growth of vanadium oxide on tin oxide. The sharp SnO_2-V_2O_5 interface indicate the epitaxial bonding driven by the low mismatch factors of the two single crystalline materials, confirmed by corresponding FFT images [14]. Given the different work functions of the two oxides and the possibility of epitaxially anchoring V_2O_5 nanostructures on SnO_2 NWs, this concept represents a viable strategy for locally modifying the electronic properties of the host materials [31].

In summary, we have developed a molecule-based catalyst assisted growth mechanism for the synthesis of single crystalline functional 1D oxides. We were able to synthesize and structurally characterize tin and iron oxides of high aspect ratio. Further a universal methodology was investigated to contact individual nanoscaled objects for the production of microcircuits, which are suitable for fast and reliable gas detection and extraction of intrinsic material properties by electrical characterisation. In addition, various shapes of oxide heterostructures based on tin oxide NWs were grown and structurally characterized for the investigation of growth phenomena and interface effects on functional properties.

Acknowledgements

Authors thank the Saarland state and federal government for providing financial assistance. The German Science Foun-

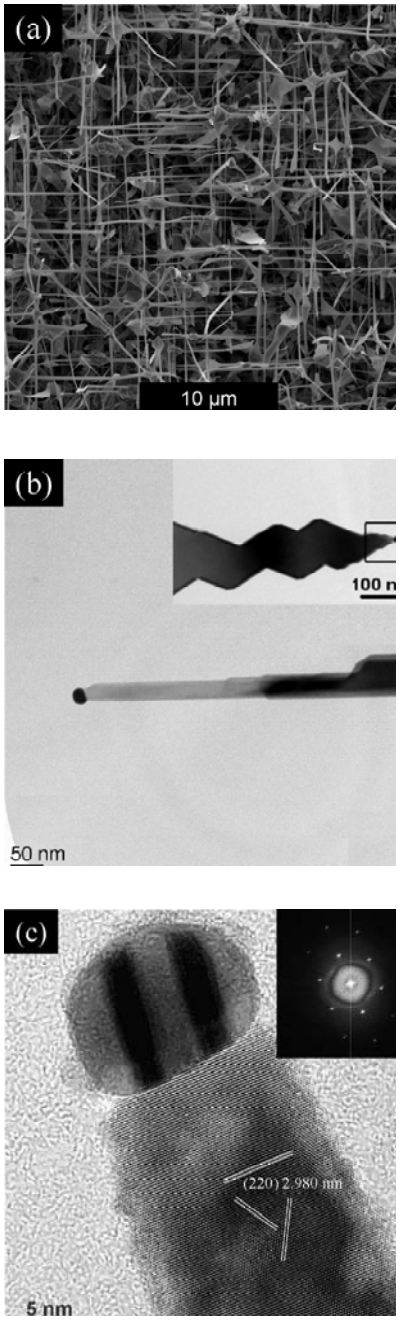

Figure 7: (a) SEM image of magnetite nanowires array. (b) TEM images of synthesized 1D Fe_3O_4 and (c) HR-TEM and FFT images of a magnetite NW close to the catalyst particle.

dation (DFG) is gratefully acknowledged for supporting our research (priority program SFB-277).

Collaboration:

F. Hernandez-Ramireza, A. Romano-Rodrigueza

a IN²UB and EME / CErMAE / CEMIC Departament d'Electronica Universidad de Barcelona, C / Marti I Franqués 1, E-08028 Barcelona, Spain

References

[1] Z. L. Wang in „ Nanowires and Nanobelts", Vol. 1 and Vol. 2 (Ed. Z. L. Wang), Springer, Berlin 2006.

[2] S. Mathur, S. Barth, H. Shen, J.-C. Pyun, U. Werner, Small 2005, 1, 713.

[3] F. Hernandez-Ramirez, A. Taracon, O. Casals, J. Rodriguez, A. Romano-Rodriguez, J. R. Morante, S. Barth, S. Mathur,T. Y. Choi, D. Poulikakos, V. Callegari, P. M. Nellen, Nanotechnology 2006, 17, 5577.

[4] F. Hernandez-Ramirez, A. Taracon, O. Casals, E. Pellicier, J. Rodriguez, A. Romano-Rodriguez, J. R. Morante, S. Barth, S. Mathur, Phys. Rev. B 2007, 76, 085429.

[5] (a) M. E. Franke, T. J. Koplin, U. Simon, Small 2006, 2, 36.

[6] M. Batzill and U. Diebold, Progress in Surface Science 2005, 79, 47.

[7] N. Bârsan, U. Weimar, J. Phys.: Condens. Matter 2003, 15, R 813.

[8] G. Heiland, D. Kohl in T. Seiyama (ed.), Chemical Sensor Technology, Vol. 1, 1–35, Kodansha, Tokyo.

[9] V. A. Henrich, P. A. Cox, The Surface Science of Metal Oxides. University Press, Cambridge 1994, 312.

[10] M. I. Baraton, L. Merhari, Nanostr. Mater. 1998, 10, 699.

[11] F. Hernandez-Ramirez, A. Tarancon, O. Casals, J. Arbitol, A. Romano-Rodriguez, J. R. Morante, Sensors Actuators B 2007, 121, 3.

[12] F. Hernandez-Ramirez, S. Barth, A. Tarancon, O. Casals, E. Pellicer, J. Rodriguez, A. Romano-Rodriguez, J. R. Morante, S. Mathur, Nanotechnology 2007, 18, 424016.

[13] F. Hernandez-Ramirez, J. D. Prades, A. Taracon, S. Barth, O. Casals, R. Jiminez-Diaz, E. Pellicier, J. Rodriguez, M. A. Juli, A. Romano-Rodriguez, J. R. Morante, S. Mathur, A. Helwig, J. Spannhake, G. Mueller, Nanotechnology 2007, 18, 495501.

[14] S. Mathur, S. Barth, Small 2007, 3, 2070.

[15] V. Schmidt, S. Senz, U. Gösele Nano Lett. 2005, 5, 931.

[16] J. H. Woodruff, J. B. Ratchford, I. A. Goldthorpe, B. C. McIntire, C. E. D. Chidsey, Nano Lett. 2007, 7, 1637.

[17] A. Q. Pankhurst, J. Connolly, S. K. Jones, J. Dobson, J. Phys. D: Appl. Phys. 2003, 36, R167.

[18] C. C. Berry, A. S. G. Curtis, J. Phys. D: Appl. Phys. 2003, 36, R198.

[19] M. Shinkai, M.- Yanase, M. Suzuki, H. Honda, T. Wakabayashi, J. Yoshida, T. Kobayshi, J. Magn. Magn. Mater. 1999, 194, 176.

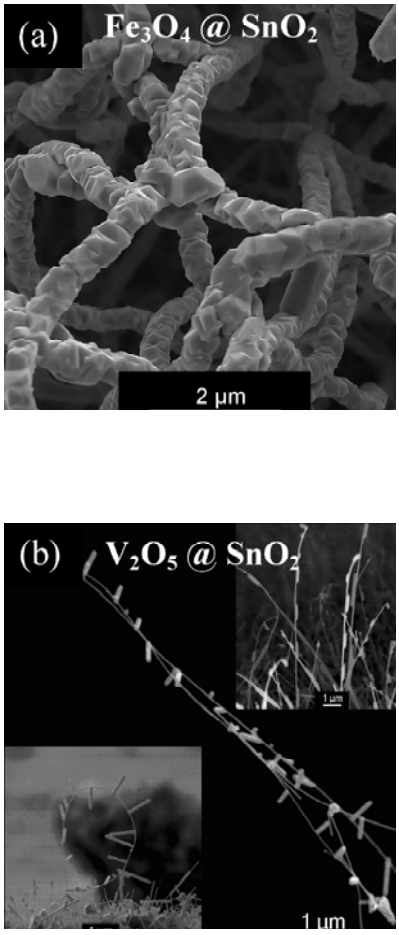

Figure 8: SEM images of (a) Fe_3O_4/SnO_2 core-shell and (b) V_2O_5/SnO_2 hierarchical nanostructures.

Mechanisms of Bonding Effected by Nanoparticles in Zirconia Coatings Applied by Spraying of Suspensions

J. Adam, M. Aslan, R. Drumm, M. Veith

[20] T. Sugimoto, in Monodisperse Particles, Elsevier, Amsterdam, Netherlands 2001.

[21] N. Nitin, L. E. W. LaConte, O. Zurkiya, X. Hu, G. Bao, J. Biol. Inorg. Chem. 2004, 9, 706.

[22] Z. Liu, D. Zhang, S. Han, C. Li, B. Lei, W. Lu, J. Fang, C. Zhou, J. Am. Chem. Soc, 2005, 127, 6.

[23] J. Wang, Q. Chen, C. Zeng, B. Hou, Adv. Mater. 2004, 16, 137.

[24] J. R. Morber, Y. Ding, M. S. Haluska, Y. Li, J. P. Liu, Z. L. Wang, R. L. Snyder, Phys. Rev. B 2006, 110, 21672.

[25] J. Bachmann, J. Jing, M. Knez, S. Barth, H. Shen, S. Mathur, U. Goesele, K. Nielsch, J. Am. Chem. Soc. 2007, 129, 9554.

[26] (a) S. Mathur, M. Veith, V. Sivakov, H. Shen, V. Huch, U. Hartmann, H. B. Gao, Chem. Vap. Depos. 2002, 8, 277; (b) S. Mathur, V. Sivakov, H. Shen, S. Barth, C. Cavelius, A. Nilsson, P. Kuhn, Thin Solid Films 2006, 502, 88; (c) S. Mathur, H. Shen, V. Sivakov, U. Werner, Chem. Mater. 2004, 16, 2449.

[27] D. M. Lind, S. D. Berry, G. Chern, H. Mathias, L. R. Testardi, Phys. Rev. B 1992, 45, 1838.

[28] (a) S. Mathur, S. Barth, U. Werner, F. Hernandez-Ramirez, A. Romano-Rodriguez, Adv. Mater. 2008, in print; (b) S. Mathur, S. Barth, Z. Phys. Chem. 2008, 222, 307.

[29] M. Bohra, N. Venkataramani, S. Prasad, N. Kumar, D. S. Misra, S. C. Sahoo, R. Krishnan, J. Magn. Magn. Mater. 2007, 310, 2242.

[30] (a) A. Vorniero, M. Ferroni, E. Comini, G. Fagkia, G. Sberveglieri, Nano Lett. 2007, 7, 3553; (b) L. Xu, Y. Su, S. Li, Y. Q. Chen, Q. T. Zhou, S. Yin, Y. Feng, Phys. Chem. B 2007, 111, 760.

[31] J. E. Evans, K. W. Springer, J. Z. Zhang, J. Chem. Phys. 1994, 101, 6222.

Mechanisms of Bonding Effected by Nanoparticles in Zirconia Coatings Applied by Spraying of Suspensions

Abstract

Zirconia coatings consisting of a mixture of coarse and fine grained zirconia powders prepared by spraying of suspensions and subsequent thermal treatment at limited temperatures (up to 500°C) are poor in adherence and in intrinsic mechanical strength. We have shown elsewhere that mechanical properties of these coatings can be improved clearly by adding a small amount of nanoscaled zirconia.

Here, the structural and the chemical development of this coating material and of the nanoparticles is examined to gain information about the underlying bonding mechanisms. The applied temperature is relatively low in comparison to the usual onset temperature of accelerated sintering. Nevertheless, the results show that diffusion controlled material transport mechanisms play their role in bonding. The condensation of surface OH groups may participate in bonding, too.